Molecular dynamics investigation of water permeation through nanopores

Rosalind Allen[a] and Jean-Pierre Hansen
Department of Chemistry, University of Cambridge, Lensfield Road, Cambridge CB2 1EW, United Kingdom

Simone Melchionna
Dipartimento di Fisica, Università "La Sapienza," P.le A. Moro 2, 00185 Roma, Italy

(Received 3 March 2003; accepted 20 May 2003)

Molecular dynamics (MD) simulations are carried out to investigate the permeation of nanometer-sized cylindrical pores connecting two reservoirs, by water molecules and by a reference Lennard-Jones fluid. Water molecules penetrate a channel of fixed length only beyond a minimum radius. Near threshold, permeation is found to be intermittent and sensitive to other physical parameters, including the polarizability of the medium (e.g., a cell membrane) embedding the channel. Once the molecules fill the pore, the confined water exhibits properties (mean density, diffusivity, hydrogen bonding) surprisingly close to those of the bulk. The intermittent behavior near the threshold is analyzed in terms of a Landau-like grand potential regarded as a function of the pore occupancy. The grand potential, which is determined using a biased sampling technique, generally exhibits two minima, associated with the ''empty'' and ''filled'' states, separated by a potential barrier (transition state). No intermittent filling of identical pores is observed in the possible case of the reference Lennard-Jones fluid over a wide range of physical conditions, pointing to the specific role of hydrogen bonding for intermittent behavior. A careful analysis of the MD-generated configurations shows that the filled state nucleates around a chain of hydrogen-bonded molecules spanning the pore. © *2003 American Institute of Physics.* [DOI: 10.1063/1.1590956]

I. INTRODUCTION

The structure and dynamical properties of highly confined fluids deviate increasingly from their bulk behavior as the characteristic dimensions of the confining volume are reduced towards the nanometre scale.[1] This paper considers the case of linear pores, where, upon decreasing the pore radius, the initially three-dimensional bulk fluid crosses over to a quasi-one-dimensional system. Physical realizations of quasicylindrical nanopores permeated by fluids include zeolites,[2] carbon nanotubes,[3,4] and ion channels through cell membranes.[5,11] As the pore narrows, very few molecules enter, and a very striking intermittent permeation of nanopores by water has recently been discovered in molecular dynamics (MD) simulations of carbon nanotubes[3,6] and subsequently in simple models of ion channels.[7,8] Although they show apparently similar behavior, the carbon nanotubes and the model ion channels are physically rather different systems. Carbon nanotubes are immersed in water, but the confining carbon surface is highly hydrophobic, and the filled state of the nanotube contains a single-file chain of water molecules. In the simple model of an ion channel presented in this work, as well as in the model of Ref. 7, the pore is well separated from the water reservoirs, and the filled state contains a much larger number of molecules, which behave in a rather bulklike manner.

Biological ion channels have a complex topology and chemical structure, involving both hydrophobic and hydrophilic residues, which depend very much on the nature of the embedding protein. The complex structure of a much studied K^+ channel has recently been resolved in great detail by x-ray diffraction,[9] and MD simulations of a very realistic model of this channel have yielded good insight into the mechanism of cation transport through the channel.[10] Similar simulations of realistic or semirealistic models, accounting in particular for the molecular ''roughness'' of the confining surface, have been reported by several groups.[11]

The present paper deals with a highly simplified model of a channel, in an effort to pin down generic features of water permeation, controlled by only a small number of physical parameters. In this model, which was introduced in Ref. 8 and will be defined in more detail in Sec. II, the channel is a cylindrical pore of finite length L and radius R spanning a dielectric continuum (the cell membrane) and connected at both ends to large reservoirs of water molecules. The present paper is restricted to a study of permeation by water, in the absence of ions (except in one particular case), as a function of three key physical parameters: namely, the radius R and length L of the channel and the dielectric permittivity ϵ of the embedding dielectric medium. Although the model is far too crude to describe specific ion channels, it is hoped that it will provide some generic insight into water permeation thresholds and the structure and dynamics of highly confined water.

The paper is organized as follows: The model, key physical parameters and MD procedures are defined in Sec. II. Section III presents results for a reference fluid, made up of Lennard-Jones atoms. The MD results for a ''realistic'' model of water, obtained over a range of values of R, L and ϵ, are presented and discussed in Sec. IV. The ''intermittent'' permeation by water is analyzed in Sec. V by calculating the

[a]Electronic mail: rja22@cam.ac.uk

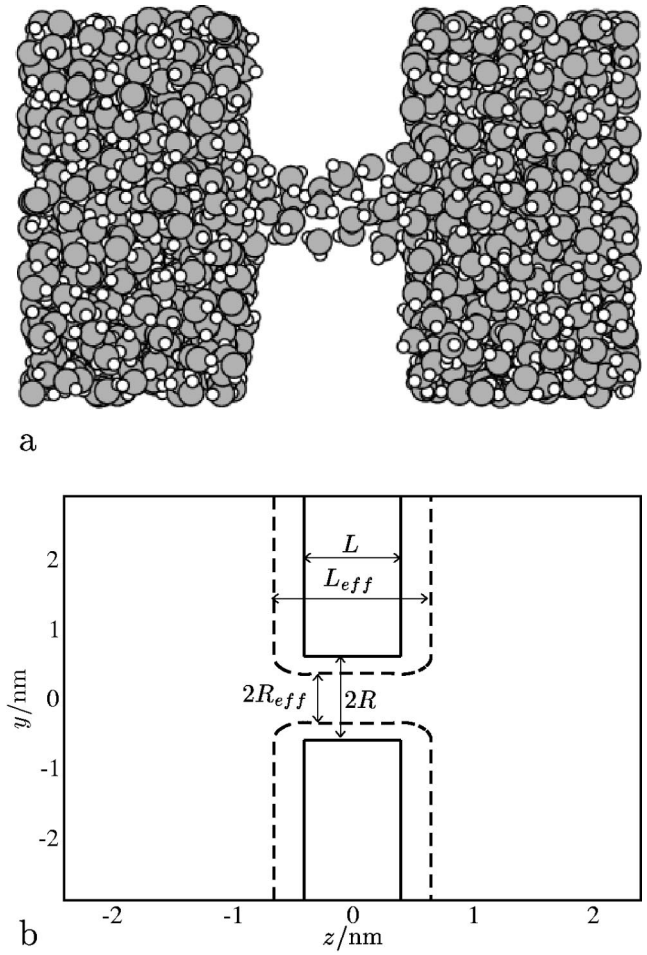

FIG. 1. (a) Snapshot of a water configuration from a simulation run with $R=0.6$ nm, $L=0.8$ nm. (b) Cut in the $x=0$ plane through a simulation cell with $R=0.6$ nm, $L=0.8$ nm, showing the position of the confining surface (solid line) and the locus of points for which $\phi_w=k_BT$ (dashed line).

free energy as a function of channel occupation, while a ''percolation'' mechanism for channel filling will be put forward in Sec. VI. Concluding remarks are made in Sec. VII.

Preliminary accounts of parts of the present work were briefly reported elsewhere.[8,12]

II. MODEL AND KEY PARAMETERS

The pore geometry which will be considered is schematically represented in Fig. 1. A cylindrical pore of length L and radius R traverses a slab of dielectric continuum representing the embedding membrane. At both ends the pore opens into ''reservoirs'' filled with water at a given density ρ and temperature T. In practice, in the MD simulations, the reservoirs are finite, containing typically up to 1000 molecules, and the whole simulation cell depicted in Fig. 1(a) is periodically repeated in all three directions, such that the left and right reservoirs are directly connected (the molecules leaving the left reservoir to the left along the z direction, coinciding with the cylinder axis, enter the right reservoir from the right according to the usual rules of periodic boundary conditions).

The water molecules interact via the standard SPC/E pair potential,[13] which involves a Lennard-Jones (LJ) potential acting between the O atoms and Coulombic interactions between sites associated with the O atoms (electric charge $-2q$) and the two H atoms (electric charge $+q$). The values of the LJ potential parameters are $\sigma=0.3169$ nm and $\epsilon=0.6502$ kJ mol^{-1} (i.e., $\epsilon/k_B=78.2$ K), while the charge $q=0.4238e$. The water molecules are rigid, with an OH bond length of 0.1 nm and an HOH bond angle of 109.5°.

The confining surface of the channel is taken to be smooth. The radial interaction between the channel surface and the water molecules is chosen to be the LJ potential between a CH_3 group and an O atom,[14] integrated over the volume surrounding an infinitely long cylindrical pore, with a wall atom number density $\rho=0.033$ Å^{-3} (Ref. 15); this yields a potential $\phi_w(r)$ experienced by water molecules that depends only on the radial distance of the O atom from the cylinder axis. The same potential, now as a function of the distance from the planar interface, is used for the membrane–water interaction, with an appropriate rounding and shifting procedure to avoid any discontinuities. The calculation of the wall–molecule interaction is described in detail in Appendix A.

Since water molecules (and ions in subsequent extensions of this work) carry electrical charges, they polarize the membrane modeled here by the dielectric slab separating the two reservoirs. Since the interface between slab, channel, or reservoir is treated as infinitely sharp, the resulting dielectric discontinuity implies that the polarization charge is entirely localized on the surface of the slab or channel.[16] The interaction between the polarization charge and the charged sites on the water molecules can be quite substantial for molecules close to the interfaces.[17] An efficient method to calculate the surface polarization charge is based on a variational formulation of the electrostatic problem,[18] and its numerical implementation is briefly described in Appendix A.

For comparitive purposes, a ''reference'' system was also considered, where the water molecule is stripped of its charged sites, so that it is reduced to ''OW'' atoms interacting solely through the LJ potential between the O sites. The interactions with the confining surfaces are left unchanged, but in the absence of charges the polarization contribution vanishes.

The key parameters in the model are the cylinder radius R and length L and the dielectric permittivity ϵ. In most simulations L was chosen to be 0.8 nm, while the radius R was varied between 0.4 and 0.7 nm. However, in view of the interaction between the channel surface and water molecules, the effective radius of the cylinder accessible to the centers of the O atoms can be estimated from the criterion that the repulsive wall–O potential be less than k_BT, as shown in Fig. 1(b). At $T=300$ K, this leads to effective radii in the range $R_{\mathrm{eff}}=0.17-0.47$ nm. Similarly the effective length of the channel is $L_{\mathrm{eff}}=1.26$ nm (for a bare length $L=0.8$ nm). These dimensions are typical of the selectivity filters of many ion channels.

The MD simulations were carried out using the package DL_PROTEIN2.1 developed by Melchionna and Cozzini.[19] Each reservoir contained typically $N=250$ (for the simulations with $\epsilon\neq1$) or $N=500$ (for simulations with $\epsilon=1$) water molecules. This number fluctuates somewhat as the chan-

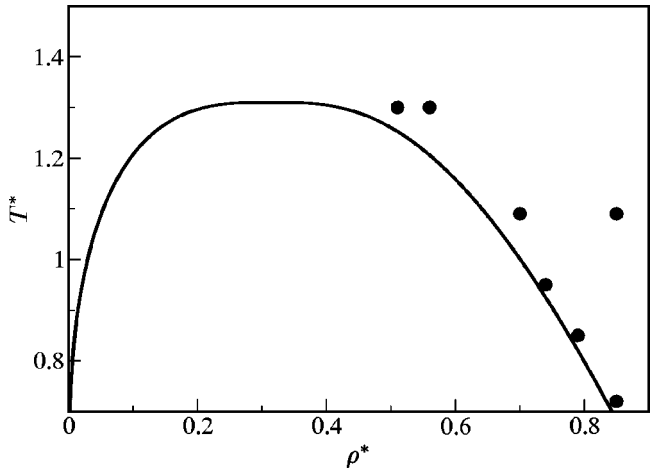

FIG. 2. Liquid–vapor phase equilibrium for the Lennard-Jones fluid, calculated from the empirical formulas given by Lotfi *et al.* (Ref. 22). Thermodynamic-state points tested for the OW system with $R=0.6$ nm and $L=0.8$ nm are marked by circles.

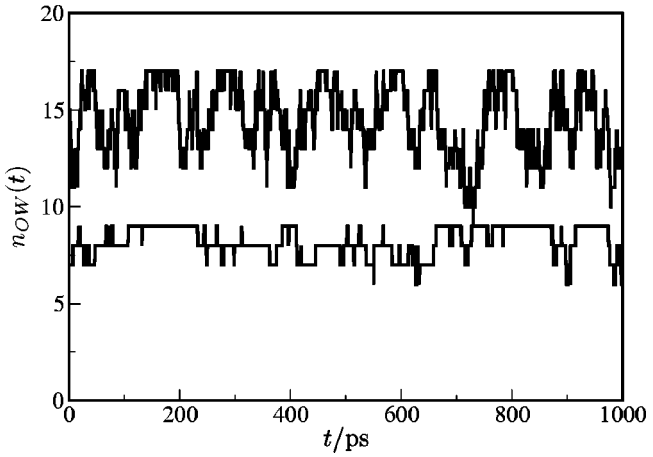

FIG. 3. Number of OW atoms inside channels of radius 0.5 nm and 0.6 nm as a function of time (in ps) for the state point $T^*=0.95$, $\rho^*=0.74$.

nel fills or empties. In order to maintain a constant density in the reservoir of 0.996 g cm^{-3}, the reservoir length along the z axis (parallel to the cylinder axis) and the z components of the atomic position vectors were regularly scaled using a version of the Berendsen barostat, while the temperature is kept constant by coupling the molecules to a Berendsen thermostat.[20] Electrostatic interactions between particles are treated using the particle mesh Ewald method.[21] The minimum image convention was used to construct the Green's function needed in the polarization charge density functional[18] and for the interaction between the particles and the polarization surface charge density (see Appendix A). The time step in the finite-difference MD algorithm was generally $\Delta t=2$ fs, and the simulations were run for up to 6 ns.

III. MOLECULAR DYNAMICS RESULTS FOR THE REFERENCE OW MODEL

Consider first the OW reference system, made up of atoms interacting via the LJ pair potential only. Under normal conditions for water ($T=300$ K, $\rho=0.996$ g cm^{-3}), the reference LJ system would be a supercritical fluid, at $T^*=k_BT/\epsilon=3.84$ and $\rho^*=\rho\sigma^3=1.06$ (Ref. 22). In order to work under physical conditions comparable to those of water (i.e., in the liquid phase, close to the triple point), the temperature must be lowered below the LJ critical temperature ($T_c^*\approx 1.36$). The interaction between the OW atoms and the confining surfaces is taken to be the same as for water. MD runs were carried out for a number of thermodynamic conditions indicated in Fig. 2, which also shows the liquid–vapor coexistence curve, according to the fitted polynomial equation of state given by Lotfi *et al.*[23] Most points were selected close to bulk liquid–vapor coexistence, so as to maximize the probability of the particles remaining liquidlike in the pore. Figure 3 shows the pore occupation—i.e., the total number $n_{OW}(t)$ of OW atoms inside the channel (with $|z|<L/2$)—as a function of time, for the system with $T^*=0.95$, $\rho^*=0.74$, and for two different pore radii. As expected, there are fluctuations in $n_{OW}(t)$ around a well-defined mean value which increases with R. An interesting observation is that the OW atoms fill the channel for all radii down to $R=0.33$ nm ($R_{\text{eff}}=0.1$ nm). Typical radial density profiles $\rho_{OW}(r)$, relative to the reservoir density, are shown in Fig. 4, for this and another state point. They indicate

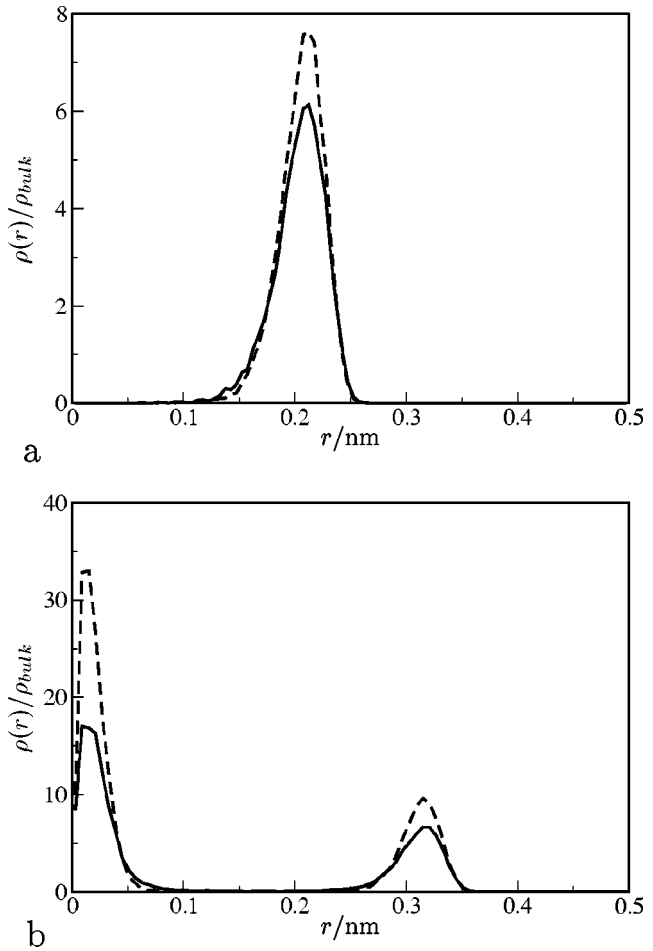

FIG. 4. Radial density profiles, relative to the reservoir density ρ_{bulk}, for OW atoms at the state points $T^*=0.95$, $\rho^*=0.74$ (solid lines) and $T^*=0.85$, $\rho^*=0.79$ (dashed lines). (a) channel radius $R=0.5$ nm, (b) $R=0.6$ nm.

TABLE I. Summary of characteristics of absorbed OW particles in pores with $L=0.8$ nm and $R=0.6$ nm.

T^*	ρ^*	Solid/fluid	D (10^{-5} cm^2 s^{-1})	$\langle n_{OW}(t)\rangle/\pi R_{\rm eff}^2 L\rho_{bulk}$
0.72	0.85	S	0	1.8
0.85	0.79	S	0	1.9
0.95	0.74	F	1	1.8
1.09	0.70	F	3	1.8
1.09	0.85	S	0	1.8
1.30	0.51	F	10	1.9
1.30	0.56	F	10	1.7
1.53	0.85	F	2	1.7

strong layering of the OW atoms inside the pore. We choose to define the mean density of particles inside the pore as $\langle n_{OW}(t)\rangle/(\pi R_{\rm eff}^2 L)$; the values are considerably larger than the bulk density of OW atoms in the reservoir (by a factor of 1.7–1.9 for the thermodynamic states investigated when $R=0.6$ nm). The fluidity of the confined atoms can be characterized by measuring the diffusion constant along the cylinder axis, using the method described in Appendix B. Although the confined particles in the three systems at the lowest temperatures are ''solid,'' showing negligible diffusion in the pore, in all other channels, diffusion constants are comparable to the reservoir value D_{res}: for example, for $T^*=0.95$, $\rho^*=0.74$, $R=0.6$ nm, $D\approx 1\times 10^{-5}$ cm^2 s^{-1} whereas $D_{res}\approx 5\times 10^{-5}$ cm^2 s^{-1}). Results for all the thermodynamic state points of Fig. 2, for pores of radius $R=0.6$ nm, are presented in Table I.

In summary, the behavior of OW atoms confined in the model nanopore is very much as expected; in particular the OW atoms appear to permeate the pore completely as soon as the effective pore radius is sufficiently large, forming a highly layered structure inside the pore.

IV. MOLECULAR DYNAMICS RESULTS FOR WATER

The behavior described in the previous section changes dramatically when the OW atoms are replaced by H_2O molecules at $T=300$ K and reservoir density $\rho=0.996$ g cm^{-3}. The number of molecules $n(t)$ inside a channel of length $L=0.8$ nm are shown as a function of time for four different cylinder radii R in Fig. 5. These data correspond to the case where membrane polarization effects are neglected: i.e., the slab region has dielectric permittivity $\epsilon=1$. For the smallest radius considered ($R=0.55$ nm), the channel shows no sign of filling over a time interval of 3 ns. The small fluctutations of $n(t)$ away from zero are caused by small numbers of water molecules entering the channel at either end. At the slightly larger channel radius $R=0.6$ nm, striking intermittent behavior is apparent, which is reminiscent of recent observations of water in carbon nanotubes[3,6] and of water in atomistically rough models of ion channels.[7] States where the channel is filled alternate in an apparently stochastic pattern with empty channel states, on a time scale of typically 1 ns. When the radius is further increased to $R=0.65$ nm, the channel appears to remain filled after initial intermittency, although it cannot be ruled out that periods in the empty state could be observed on longer time scales. Finally, at $R=0.7$ nm, the channel appears to remain filled throughout, with a mean density of 0.034 Å^{-3} comparable to the bulk density in the reservoir, 0.033 Å^{-3}.

The threshold radius for intermittent behavior is sensitive to membrane polarization effects: the latter are expected to lower the electrostatic energy of a water molecule inside the channel, thus favoring water permeation for lower pore radii. The situation is illustrated in Fig. 6 which compares occupation number histories for pores with channel radius $R=0.525$ nm and two values of the dielectric permittivity of the embedding slab ($\epsilon=1$ and 10). Clearly polarization ef-

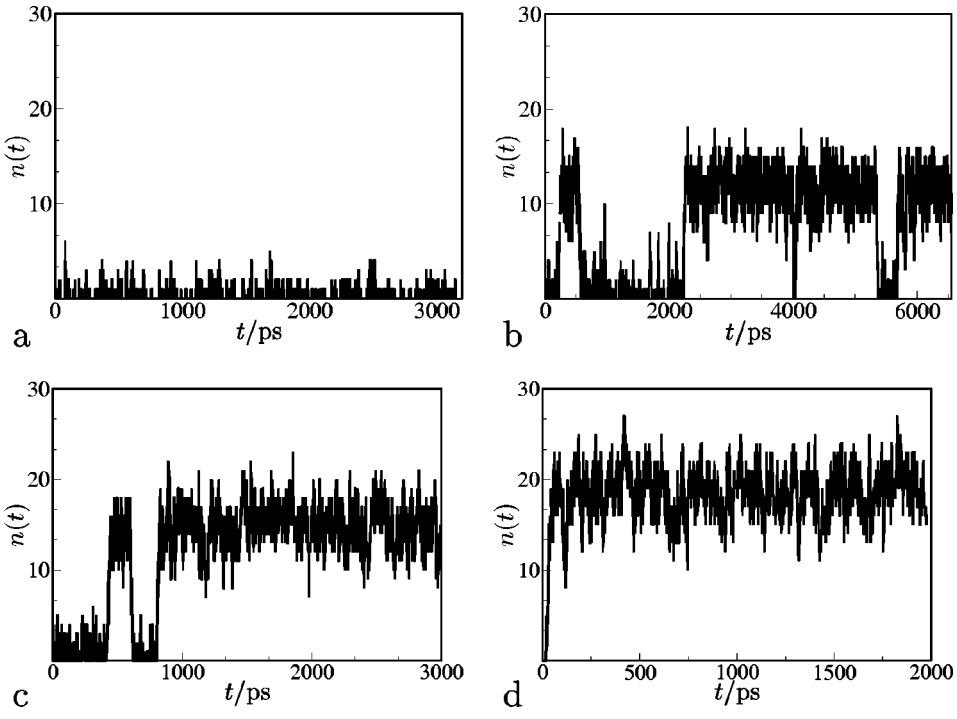

FIG. 5. Number $n(t)$ of water molecules inside channels with $\epsilon=1$ of length $L=0.8$ nm and radii (a) $R=0.55$ nm, (b) $R=0.6$ nm, (c) $R=0.65$ nm, and (d) $R=0.7$ nm, as a funtion of time (in ps); the durations of the four runs vary.

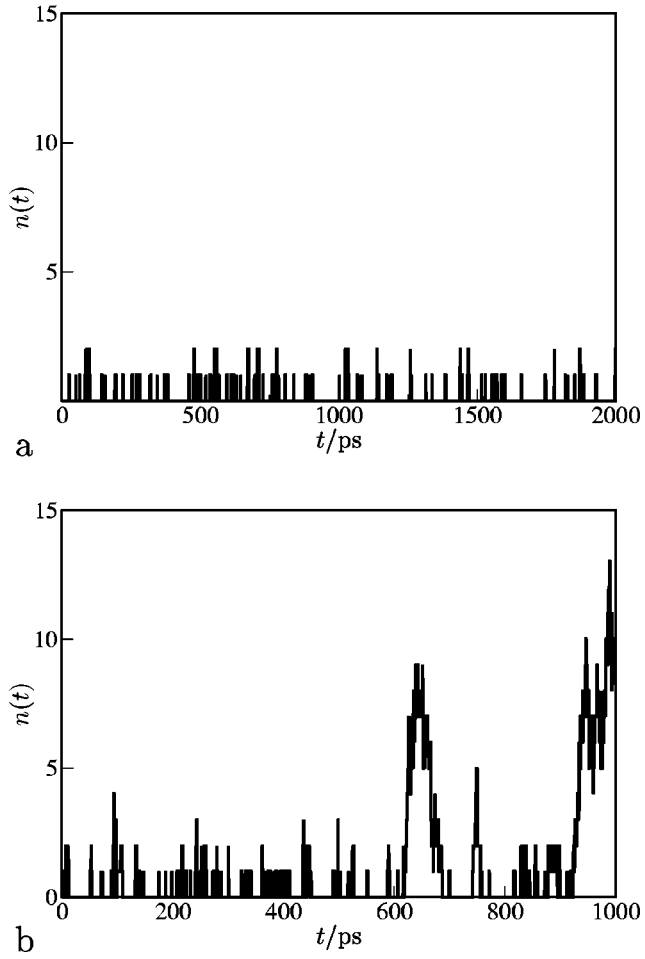

FIG. 6. Number $n(t)$ of water molecules inside channels of length $L=0.8$ nm and radius $R=0.525$ nm (a) $\epsilon=1$, (b) $\epsilon=10$. Note the simulation run is longer in (a).

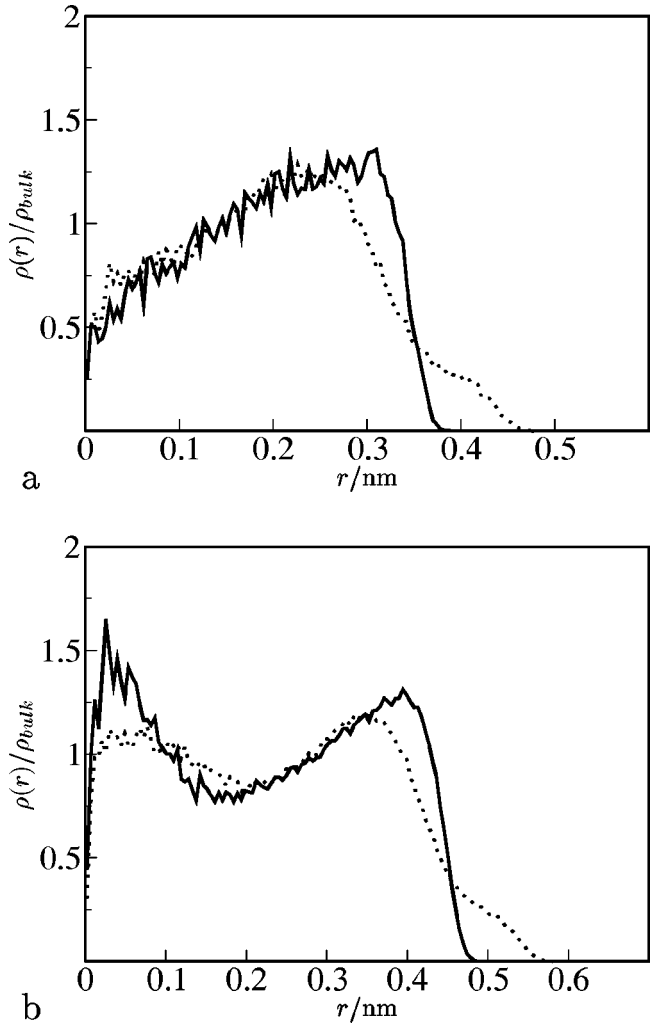

FIG. 7. Radial density profiles $\rho(r)$, relative to the reservoir density ρ_{bulk} for O atoms (solid lines) and H atoms (dotted lines) of water in channels of length $L=0.8$ nm and radii (a) $R=0.6$ nm and (b) $R=0.7$ nm. Averages are taken only over times when the channel is filled.

fects lower the threshold of intermittent behavior or filling behavior to smaller radii. These simulations were carried out on smaller systems, with a total of 534 water molecules, rather than 1068 molecules as in all other runs, due to the additional time needed to compute the wall polarization effects. We note that channel permeation was found to be also sensitive to the reservoir size in this regime where the reservoir is rather small.

The time scale of the intermittent behavior is clearly very sensitive to the control parameters of the model in the vicinity of the threshold. Since this time scale is of the order of the total length of the MD runs (typically a few ns), the distinction between intermittent, empty, and filled states is of course not completely well defined. This will, however, be clarified by the free energy analysis to be discussed in Sec. V.

One would also expect water permeation to be strongly influenced by the presence of ions, in particular small cations, which are surrounded by long-lived hydration shells in the bulk. To examine the effect of ions on permeation, MD simulations were carried out with a K^+ ion fixed on the axis in the middle of a channel of radius $R=0.5$ nm, which would remain empty of water molecules in the absence of the ion. With the K^+ ion present, the channel was found to be rapidly filled by water molecules, with an average occupation number $\langle n\rangle \approx 6.5$. In fact, water molecules were found to penetrate channels with R as small as 0.3 nm ($R_{\text{eff}}=0.07$ nm) under these circumstances.

The intermittent behavior shown in Fig. 5 is reminiscent of that observed for the narrower carbon nanotubes of Refs. 3 and 6 and for a more ''realistic'' model of an ion channel in Ref. 7.

The MD simulations allow a more detailed analysis of the structure of the water in the pores. Radial density profiles of the centres of the O and H atoms of the H_2O molecules are shown in Fig. 7 for the channels with $R=0.6$ nm and $R=0.7$ nm. These profiles were averaged over the total length L of the channel. For intermittent filling, the profiles were averaged over filled configurations only. The various profiles are seen to be rather flat compared to the highly structured profiles of the OW reference system, shown in Fig. 4. The mean density of water molecules inside the channel is always close to the reservoir value, suggesting that the molecules fill all the available volume. The profiles turn out to be surprisingly insensitive to polarization effects—i.e., to the value of the dielectric permittivity ϵ of the confining slab.

TABLE II. Properties of water dynamics for pores with $L=0.8$ nm and $\epsilon=1$. Averages are taken only during times when the channels were filled.

R (nm)	D (10^{-5} cm^2 s^{-2})	Crossing rate (ps^{-1})
0.6	4	0.1 ± 0.04
0.65	4	0.2 ± 0.05
0.7	4	0.1 ± 0.05

An analysis of the hydrogen bond network inside the filled channels, similar to the analysis of Lee, McCammon, and Rossky for water near a smooth planar substrate,[24] is described in detail in Ref. 12. The average number of hydrogen bonds per molecule [defined according to an energetic criterion requiring the interaction between two water molecules to be less than -9.42 kJ mol^{-1} (Ref. 25)] was plotted as a function of the radial distance r from the cylinder axis. This analysis showed that the water molecules inside the pore deviate from their bulk configuration, so as to strengthen their hydrogen bond network close to the surface. This tendency was also observed by Lee *et al.* for the planar geometry.[24] It is also to be noted that membrane polarization (i.e., choosing $\epsilon>1$) has practically no effect on these hydrogen bond profiles.

The self-diffusion constant D of water molecules along the channel axis is measured by plotting the mean-square displacement in the z direction as a function of time, for molecules inside the channel, as described in Appendix B. Values for several pore radii are given in Table II, together with the rate at which water molecules successfully cross the channel from end to end. The axial diffusivity of water molecules during periods when a channel is full is surprisingly insensitive to R and ϵ and comparable to bulk diffusion. The number of crossings are comparable in the two directions, so there is no net flux of water, as expected in an equilibrium simulation.

The overall picture that emerges from the simulations is that water confined to narrow pores behaves in a surprisingly similar way to bulk water, in terms of mean density and diffusivity. This high ''fluidity'' of water in pores agrees qualitatively with recent surface force apparatus measurements of highly confined water films.[26]

V. FREE ENERGY ANALYSIS OF INTERMITTENT PERMEATION

The striking intermittent permeation of the model channel by water molecules over a range of pore radii can be analyzed in terms of a free energy depending on an appropriate ''reaction coordinate,'' in analogy with chemical reactions or with crystal nucleation. Figures 5 and 6 show that, in the intermittent mode, the channel remains in either the empty or the filled state over substantial time intervals. This means that a properly defined thermodynamic potential depending on occupation number n (playing the role of the reaction coordinate) should exhibit two minima separated by a barrier (the ''transition state''). The determination of such a thermodynamic potential is the objective of the present section. In order to analyze free energy changes in this way, it is important to specify the relevant statistical mechanical ensemble. The scaling of the z components of the position vectors using a modified Berendsen barostat, described in Sec. II, maintains the water molecules deep in the reservoir regions at constant average density. This is equivalent to fixing the chemical potential of the water in the reservoir, and thus the region near the channel is effectively simulated in the grand canonical ensemble. The relevant thermodynamic potential for a subsystem consisting of just the region near the pore is therefore $\Omega=U-TS-N\mu$, where U is the internal energy of the subsystem, S its entropy, μ the chemical potential of water in the reservoir, and N the number of water molecules in the subsystem (note that this is not the same as the number in the channel, since the channel surroundings are also included). In practice, the subsystem is defined to be the region where $|z|\leqslant L_{\mathrm{eff}}/2+X$, where $X=0.52$ nm.

The contribution of the interactions of a particular particle to the total internal energy is one of the outputs of the simulation. These contributions are summed over all particles in the subsystem region to obtain the subsystem internal energy U. Note that interactions between particles of the subsystem and of the reservoir are thus included in U, so as to reduce surface effects at the subsystem–reservoir interface.

The chemical potential μ of the SPC/E water model under these conditions of temperature and density has been calculated by several authors using different methods, with good agreement between their results. The excess component μ_{ex} is given by Shelley and Patey[27] as $\mu_{ex}=-29.1$ kJ mol$^{-1}=-11.67k_BT$. Adding the ideal contribution gives $\mu=-15.01k_BT$.

The grand potential of the subsystem is to be computed as a function of the ''order parameter'' n, the total number of water molecules inside the channel. $\Omega(n)$ is defined like a Landau free energy, as the weighted volume of phase space accessible to systems having exactly n molecules within the channel:

$$\Omega(n)=-kT\ln\Xi(n), \tag{1}$$

where the constrained grand partition function is

$$\Xi(n)=\sum_{N=0}^{\infty}\frac{\mathrm{e}^{\beta\mu N}}{N!\Lambda^{3N}}\int d\mathbf{r}^N\,\mathrm{e}^{-\beta V_N(\{\mathbf{r_i}\})}\delta(n'(\{\mathbf{r_i}\})-n). \tag{2}$$

On the right-hand side (RHS) Λ is the thermal de Broglie wavelength of water molecules, $V_N(\{\mathbf{r_i}\})$ is the total interaction energy (including particle–particle and particle–wall interactions) of the subsystem, for a configuration $\{\mathbf{r_i}\}$ and $n'(\{\mathbf{r_i}\})$ is the function giving the number of particles inside the pore for that configuration. The integration over all particle coordinates $d\mathbf{r}^N$ is taken to include the orientational degrees of freedom of the water molecules. The grand potential $\Omega(n)$ is directly related to the probability $P(n)$ that the subsystem has a value n of the order parameter according to

$$\frac{\Omega(n)}{k_BT}=-\ln P(n)+C, \tag{3}$$

where C measures the total volume of phase space accessible to the subsystem.

To sample $P(n)$ efficiently for "rare" (low probability) values of n, we introduce a biasing potential. Since the gradient of this potential will be required to calculate forces in the MD simulations, it is necessary to let n vary continuously rather than by discrete steps. We redefine n as a smoothed coordinate (or order parameter):

$$n=\sum_{i=1}^{N} f(\mathbf{r_i}). \tag{4}$$

The weighting function f is defined to be unity when molecule i is inside the channel, to go to zero outside, and to vary smoothly near the two entrances of the channel. This means that the gradient of f is nonzero only in the vicinity of the channel entrances, and so the "artificial" forces resulting from the n-dependent biasing potential will act only in these regions. A convenient weighting function is

$$f(\mathbf{r_i})=g(r_i)h(z_i), \tag{5}$$

where $\mathbf{r_i}$ is the position vector of the O atom in the ith water molecule, $r_i=\sqrt{x_i^2+y_i^2}$ is the radial distance from the cylinder axis, and the functions g and h are defined as

$$g(r)=\frac{1}{2}\{1-\tanh[\xi(r-R)]\}, \tag{6}$$

$$h(z)=\frac{1}{2}\left\{1\pm\tanh\left[\xi\left(z\pm\frac{L_{\mathrm{eff}}}{2}\right)\right]\right\}. \tag{7}$$

Here, the parameter ξ determines the steepness of the weighting function (in the MD simulation $\xi=2\ \text{Å}^{-1}$ was chosen), and the plus and minus signs in Eq. (7) are for $z<0$ and $z>0$, respectively. Note that the weighting function involves the effective channel length L_{eff} rather than the nominal length L, a choice which proves more convenient for the biasing procedure, to be described below. This means that the average occupation numbers $\langle n\rangle$ in the "empty" and "filled" states of the channel are shifted upwards, since water molecules near the entrance are now included in the count, but the intermittent pattern in Figs. 5 and 6 is unaffected, except for a uniform upwards shift. For example the mean occupation number $\langle n\rangle\approx 18$ in Fig. 5(d) increases to $\langle n\rangle\approx 34$ when the definition (4) is used.

Simulation methods for the calculation of Landau free energy profiles [$\Omega(n)$ in the present case] are well established.[28] They are generally implemented in conjunction with Monte Carlo simulations, but the same principles apply to MD simulations, as used in this paper. The grand potential profiles can be calculated from a standard simulation run, within an additive constant C, using Eq. (3). However, the sampling of less probable values of the order parameter n ("rare events") may be very poor with this method, making it impossible to determine $P(n)$ with good accuracy in that range.

The solution to this problem is to force sampling of the less probable values of n by applying an artificial, or "biasing," potential $W(n)$, in addition to the usual Hamiltonian for the system. One may write the (unbiased) average of some quantity $Y(\{\mathbf{r}^N\})$ as

$$\langle Y\rangle=\frac{\Sigma_{N=0}^{\infty}e^{\beta\mu N}\int d\mathbf{r}^N Y(\{\mathbf{r}^N\})e^{-\beta V_N(\{\mathbf{r}^N\})}e^{-\beta W(n)}e^{+\beta W(n)}/(N!\Lambda^{3N})}{\Sigma_{N=0}^{\infty}e^{\beta\mu N}\int d\mathbf{r}^N e^{-\beta V_N(\{\mathbf{r}^N\})}e^{-\beta W(n)}e^{+\beta W(n)}/(N!\Lambda^{3N})}. \tag{8}$$

Defining $V'=V+W$, which is the total potential energy of the biased system, Eq. (8) can be rewritten as

$$\langle Y\rangle=\frac{\Sigma_{N=0}^{\infty}e^{\beta\mu N}\int d\mathbf{r}^N Y e^{-\beta V'}e^{+\beta W(n)}/(N!\Lambda^{3N})}{\Sigma_{N=0}^{\infty}e^{\beta\mu N}\int d\mathbf{r}^N e^{-\beta V'}e^{+\beta W(n)}/(N!\Lambda^{3N})}. \tag{9}$$

This may be expressed in terms of averages over the biased ensemble:

$$\langle Y\rangle=\frac{\langle Y e^{+\beta W}\rangle_{bias}}{\langle e^{+\beta W}\rangle_{bias}}. \tag{10}$$

The probability of obtaining a particular value of n, $P(n^*)$, is given by $P(n^*)=\langle\delta(n-n^*)\rangle$. Using Eq. (10), we obtain the relation

$$P(n^*)=\frac{\langle\delta(n-n^*)e^{+\beta W(n)}\rangle_{bias}}{\langle e^{+\beta W(n)}\rangle_{bias}}=\frac{e^{+\beta W(n^*)}P(n^*)_{bias}}{\langle e^{+\beta W(n)}\rangle_{bias}}. \tag{11}$$

Thus the grand potential for the unbiased ensemble can be written in terms of the probability obtained from a biased simulation:

$$\begin{aligned}\Omega(n)/kT&=-\ln P(n)+C\\&=-\ln P(n)_{bias}-W/k_BT\\&\quad+\ln\langle e^{+\beta W(n)}\rangle_{bias}+C.\end{aligned} \tag{12}$$

The penultimate term on the RHS of Eq. (12) is a biasing-potential-dependent constant which may be combined with C into a single constant A:

$$\Omega(n)/kT=-\ln P(n)_{bias}-W/k_BT+A. \tag{13}$$

In the case where one is interested in an unbiased average for a fixed value $n=n^*$, the equation analogous Eq. (8) is

$$\langle Y(n^*)\rangle = \frac{\Sigma_{N=0}^{\infty} e^{\beta\mu N} \int d\mathbf{r}^N Y(\{\mathbf{r}^N\})\,\delta(n-n^*) e^{-\beta V'} e^{\beta W(n)}/(N!\Lambda^{3N})}{\Sigma_{N=0}^{\infty} e^{\beta\mu N} \int d\mathbf{r}^N \delta(n-n^*) e^{-\beta V'} e^{\beta W(n)}/(N!\Lambda^{3N})}. \tag{14}$$

Equation (14) will be important when evaluating, for example, the internal energy as a function of n.

The aim is to construct the biasing potential W so as to force the system to sample evenly values of the order parameter within a certain range or ''window.'' The grand potential profile within that window can then be obtained using Eq. (12), apart from the constant A, which is different for each window and which can be determined by matching up different windows to make a continuous profile. The practical implementation of the biasing procedure is described in Appendix C.

Grand potential profiles were computed using this method for a range of different channel geometries. Results are shown in Fig. 8 for four geometries, together with tenth-order polymonial fits to the data (cf. Appendix C). All profiles are for $\epsilon = 1$ (nonpolarizable membrane). The profiles exhibit a ''double-well'' structure, indicative of a two-state system, the two states being physically associated with ''empty'' and ''full'' channels. The positions of the minima in $\Omega(n)$ associated with the filled and empty states, n_f and n_e, and that of the maximum corresponding to the transition state, n_t, are listed in Table III for all the cases that were simulated. Table III also shows the grand potential difference between the empty and transition states, $\Delta\Omega_{te}$, between the filled and transition states, $\Delta\Omega_{tf}$, and between the filled and empty states, $\Delta\Omega_{fe}$. These characterize the grand potential barriers to the filling and emptying processes.

For the pore of radius $R = 0.6$ nm and length $L = 0.8$ nm, the profile $\Omega(n)$ shown in Fig. 8(a) exhibits two minima, one corresponding to the ''empty'' state at $n = 5.1$ (the minimum is not at $n = 0$ because of the definition of the weight function, which includes some molecules just outside the ''nominal'' channel) and the other to the ''full'' state at $n = 22.6$. The maximum in $\Omega(n)$ is at $n = 11.7$, much closer in n to the empty than to the filled state, suggesting that the transition state for the process has relatively few molecules in the pore. The difference in Ω between the two states is $3.1 k_B T$, and the barriers for the filling and emptying processes (given in Table III) are a few $k_B T$, as expected in the context of the unbiased simulation data of Fig. 5(b), for which this pore shows intermittent switching between the two states.

The wider pore, of radius 0.7 nm, remains in the filled state in the unbiased simulation of Fig. 5(c). This is unsurprising in the context of the grand potential profile of Fig. 8(b), which shows that the filled state is favored over the empty by $8.5 k_B T$, with a barrier to filling of only $0.3 k_B T$ but of $8.7 k_B T$ for emptying. Once again the transition state contains relatively few molecules: in fact the data in Table III shows that the ratio n_t/n_f is generally around 0.5, except for the channel with $R = 0.55$ nm and $L = 0.8$ nm, which appears to be somewhat anomalous.

The existence of stable filled states for long or narrow channels is difficult to determine using unbiased simulations, since the time scale of intermittency in these channels is expected to be much longer. Figure 8(c) shows $\Omega(n)$ for a longer channel, with $R = 0.6$ nm and $L = 1.0$ nm: there is in-

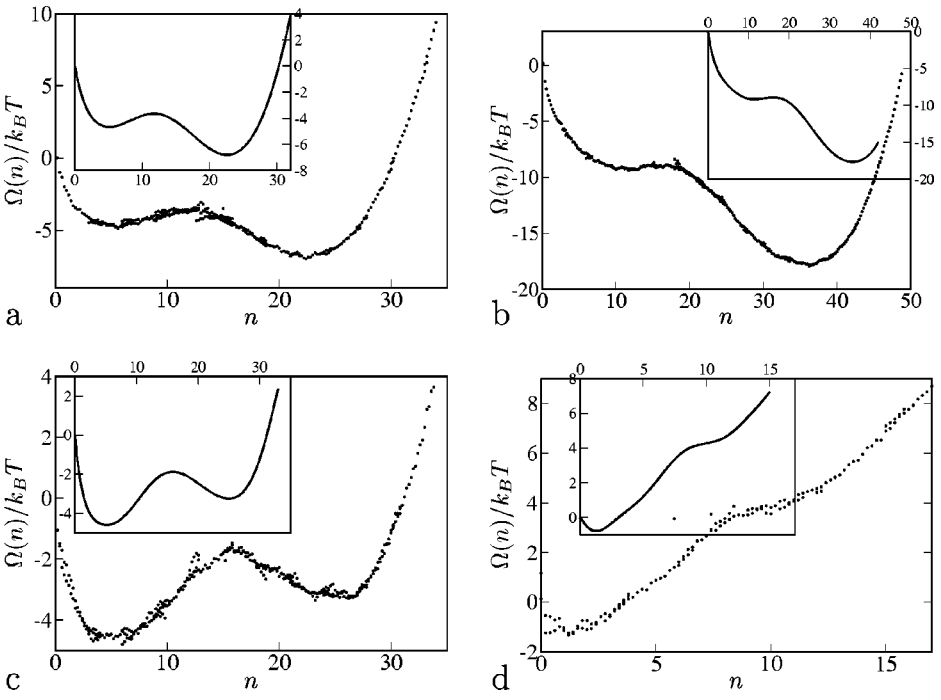

FIG. 8. Grand potential profiles $\Omega(n)/k_BT$, for four different channel geometries. (a) $L = 0.8$ nm, $R = 0.6$ nm, (b) $L = 0.8$ nm, $R = 0.7$ nm, (c) $L = 1.0$ nm, $R = 0.6$ nm, (d) $L = 0.8$ nm, $R = 0.5$ nm. The main plots show the simulation data and the insets the fitted polynomial profiles.

TABLE III. Positions of minima and maximum in $\Omega(n)$ as well as grand potential differences for various channel geometries.

R (nm)	L (nm)	n_{empty}	n_{trans}	n_{full}	$\Delta\Omega_{te}/k_BT$	$\Delta\Omega_{tf}/k_BT$	$\Delta\Omega_{fe}/k_BT$
0.55	0.7	2.4	8.9	17.7	1.6	1.3	0.3
0.55	0.8	3.1	12.8	14.5	3.5	0.1	3.4
0.6	0.8	5.1	11.7	22.6	1.0	3.1	−2.1
0.6	0.7	5.3	9.3	20.6	0.2	3.9	−3.8
0.6	1.0	5.2	15.9	25.0	2.7	1.4	1.4
0.65	0.8	7.6	14.9	28.6	1.1	5.1	−3.9
0.7	0.8	11.4	16.1	35.9	0.3	8.8	−8.5

deed a stable filled state, although the empty state is thermodynamically more favorable and there is a large grand potential barrier to filling. Results for a narrower channel, with $R=0.5$ nm and $L=0.8$ nm, are shown in Fig. 8(d). In this case, the minimum corresponding to the filled state has been lost and no intermittency is expected even in an extremely long simulation. Further calculations show that this is also the case for the channel with $R=0.5$ nm and $L=0.7$ nm.

We note that free energy curves are also shown for a carbon nanotube in Refs. 3 and 6, but these are rather different since they correspond to single-file permeation.

The observations of Sec. III that the OW reference model behaves very differently to SPC/E water are borne out by the grand potential profile for the OW fluid in a pore of radius $R=0.6$ nm (at $T^*=0.95$ and $\rho^*=0.74$), shown in Fig. 9. Here $\Omega(n)$ has a very deep minimum for the filled state and there is no stable empty state or free energy barrier.

Once grand potential profiles have been determined, the equilibrium probabilities $P(\text{full})$ and $P(\text{empty})$ can be predicted for a particular channel. From Eqs. (1) and (3) we obtain

$$\frac{P(\text{full})}{P(\text{empty})}=\frac{\Xi(\text{full})}{\Xi(\text{empty})}=\frac{\int_{n^\dagger}^{\infty}e^{-\beta\Omega(n)}dn}{\int_{0}^{n^\dagger}e^{-\beta\Omega(n)}dn}, \tag{15}$$

where $n^\dagger$ is the value of n at the transition state [maximum of $\Omega(n)$]. For the three channels with stable minima in Fig. 8 we find $P(\text{full})=0.892$ ($R=0.6$ nm, $L=0.8$ nm), 0.999 ($R=0.7$ nm, $L=0.8$ nm), and 0.239 ($R=0.6$ nm, $L=1.0$ nm); the trend is according to expectations.

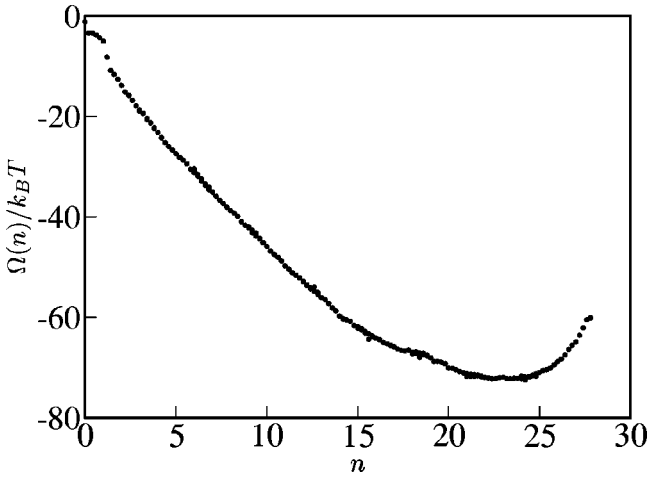

FIG. 9. Grand potential profile $\Omega(n)$ for OW particles filling a channel of radius 0.6 nm and length 0.8 nm for the state point $T^*=0.95$, $\rho^*=0.74$.

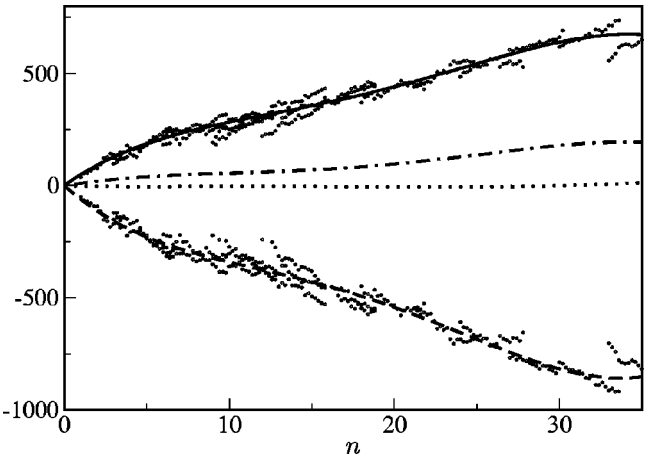

FIG. 10. Components of $\Omega(n)$ (in units of k_BT), for the channel with $R=0.6$ nm and $L=0.8$ nm. Dotted line: $\Omega(n)$. Dashed line: $U(n)$. Solid line: $-\mu N(n)$. Dot-dashed line: $-TS(n)$. Lines show fitted profiles, shifted vertically by their values at $n=0$. Data points for $U(n)$ and $-\mu N(n)$ (also shifted vertically) are shown by circles.

It is interesting to break up the grand potential of the subsystem into its three contributions:

$$\Omega(n)=U(n)-TS(n)-N(n)\mu. \tag{16}$$

The ''subsystem'' is defined as the region of the simulation box near the pore, such that $|z|\leqslant L_{\text{eff}}/2+X$, where $X=0.52$ nm (the trends described below are unaffected if X is increased to 0.77 nm). The remaining part of the simulation box acts as a reservoir, and the chemical potential μ is taken to be that of bulk SPC/E water.[27] $U(n)$ is the mean internal energy of the subsystem when there are exactly n molecules inside the channel and is evaluated using Eq. (14). It includes the LJ and Coulombic interactions between water molecules and the particle–wall interactions. The water–water interactions across the dividing surfaces $z=\pm(L_{\text{eff}}/2+X)$ (i.e., between molecules in the subsystem and in the reservoir) are included in the internal energy. Similarly, $N(n)$ is the mean total number of water molecules in the subsystem when there are n molecules in the pore. Both $U(n)$ and $N(n)$ are calculated during the ''biased'' runs and fitted to fourth-order polynomials in n using a similar procedure to that described in Appendix C. Equation (16) finally allows the entropy $S(n)$ to be extracted.

The four thermodynamic quantities $\Omega(n)$, $U(n)$, $-\mu N(n)$, and $-TS(n)$ are plotted in Fig. 10. The grand potential profile $\Omega(n)$, which changes by only a few k_BT between the empty and filled states, is seen to result from a competition between much larger changes in its components. Figure 10 clearly shows that the energetic component strongly favors channel filling, while the entropic and chemical potential contributions are strongly unfavorable. Although the entropic contribution to Ω is smaller than the chemical potential and energetic parts, it is nevertheless essential to the intermittent filling and emptying behavior. In fact $C=U-\mu N$ does not exhibit a double minimum, but

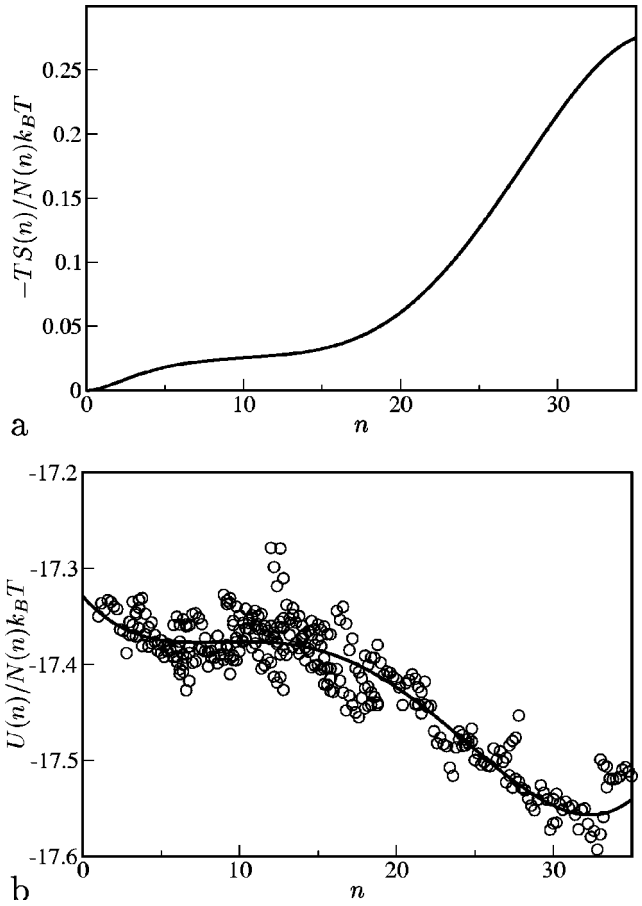

FIG. 11. (a) $-Ts$, where s is the entropy per molecule in the subsystem (absolute value is undetermined) and (b) internal energy per molecule in the subsystem. Solid lines show profiles fitted by a fourth-order polynomial. Data is for the pore with $R=0.6$ nm and $L=0.8$ nm, and the subsystem is defined by $|z|\leqslant L_{\mathrm{eff}}/2+X$, where $X=0.52$ nm.

rather a single minimum for large values of n. The role of entropy appears to be to stabilize the *empty* state and to provide the barrier for channel filling. This is confirmed by the data in Fig. 11(a), which shows the variation of the entropy $-Ts=-TS/N$ per molecule in the subsystem with n (for the same channel geometry); s decreases as the channel fills, suggesting that moving a water molecule into the pore is entropically unfavorable. Figure 11(b) shows the energy per molecule, $u=U/N$, which is always well above its bulk value of $-18.32k_BT$, presumably because molecules near the interfaces are less favorably hydrogen bonded than those in the reservoir, but decreases as the number n of molecules inside the channel increases. We note that the rather scattered data in Figs. 10 and 11(b) reflect the fact that in comparing the subsystem internal energy U or number of particles N for different values of n one is in effect calculating small differences between large numbers.

A tentative conclusion of the trends shown in Fig. 11 is that water molecules inside the pore form a more structured, energetically stronger, but entropically less favorable, hydrogen bond network than the subsystem average (which includes those molecules next to the planar surfaces). This points to the existence of a bulklike hydrogen bond network inside the pore, as already suggested by the mean density

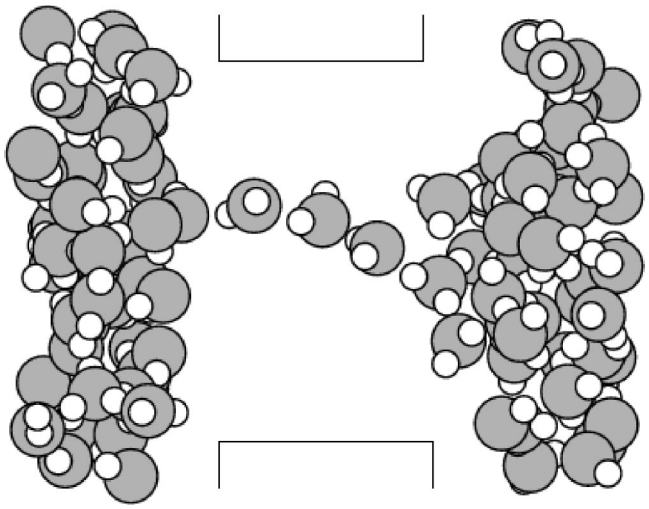

FIG. 12. Snapshot of a ''percolating cluster'' from a biased simulation run with $R=0.6$ nm, $L=0.8$ nm. Only the water molecules near the pore are shown. The positions of the confining walls are indicated.

inside the channel, which is very close to the bulk value, and by the bulklike diffusivity. These conclusions are reinforced by an analysis of the components of the energy per molecule inside the pore (i.e., counting only those molecules whose O atoms have $|z|\leqslant L_{\mathrm{eff}}/2$). As the channel fills, the Coulombic and van der Waals energies per molecule approach those of the bulk, as does the total energy per molecule.

These findings are at the basis of a simple phenomenological model, described in Appendix D.

VI. POSSIBLE FILLING MECHANISM

A close examination of configurations of water molecules inside the channel suggests that the formation of a single, unbroken (''percolating'') chain of hydrogen-bonded molecules spanning the whole pore generally precedes a rapid filling of the channel. In other words, channel filling ''nucleates'' around a percolating cluster. Another hint in that direction is the observation that the transition state in the filling process occurs for relatively small values of n (cf. Table III). An example of such a percolating cluster is shown in Fig. 12. The observations may be quantified by analyzing the collection of molecular configurations generated by the biased sampling procedure for different values of n. Using the same energetic definition of a hydrogen bond, the probability of finding a percolating cluster of water molecules across the channel can be measured from the collection of configurations having a particular value of n, obtained from the biased sampling procedure. Results for two pore geometries are shown in Fig. 13, together with the corresponding grand potential profiles, which have been scaled and shifted in the vertical direction for clarity. When n is small, there is never a percolating cluster, and when n is large enough, there is almost always one present. The crossover between ''percolating'' and ''nonpercolating'' behavior occurs in the region around the grand potential barrier, and interestingly the point at which the probability of percolation is 1/2 is close to the maximum of $\Omega(n)$. Results for the other channel geometries listed in Table III give similar results for cases when

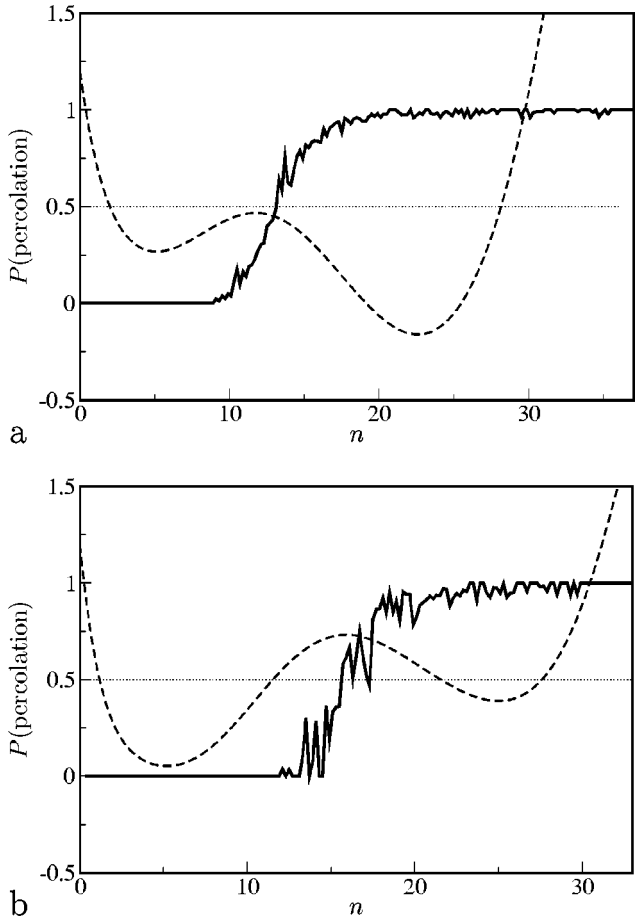

FIG. 13. Probability of finding an unbroken chain of water molecules through the pore (''percolation''), as a function of n. The dashed line shows a scaled version, shifted vertically, of the grand potential profile $\Omega(n)$. (a) $R=0.6$ nm, $L=0.8$ nm; (b) $R=0.6$ nm, $L=1.0$ nm.

the barriers to both the filling and emptying processes are of the order of a few k_BT (i.e., consideration of a nucleation mechanism is appropriate). These observations are strong evidence for the ''percolating nucleus'' mechanism for channel filling.

VII. CONCLUSION

Molecular dynamics simulations have been used to investigate a highly simplified model for the selectivity filter of an ion channel and to characterize the permeation of such channels by water molecules. For given water–water and water–wall interactions, the cylindrical model channel is entirely characterized by three physical parameters: the radius R and length L of the pore and the dielectric permittivity ϵ of the membrane spanned by the channel. Most simulations were carried out for $L=0.8$ nm and several values of R and ϵ. The key conclusions of the investigation are the following:

(a) The permeation of a pore of fixed length by water is very sensitive to the pore radius. For very narrow channels, water molecules are excluded from the pore, but as the radius increases beyond a threshold value, permeation occurs. Just above the threshold, the permeation is intermittent: i.e., the channel switches back and forth between ''empty'' and ''filled'' states on a nanosecond time scale. The transitions between the two states appear to be stochastic. As R increases, the duration of the periods in the filled state increases relative to that of the empty state until the channel remains filled, on the time scale of the MD simulations. The threshold radius R for intermittent behavior is sensitive to the permittivity ϵ of the membrane; when the latter is polarizable ($\epsilon>1$) intermittent permeation sets in for a smaller radius; in other words permeation is enhanced by dielectric polarization of the medium surrounding the pore. Both the observed intermittent permeation and the sensitivity to membrane polarization effects are reminiscent of observations made in simulations of water permeation for a more detailed model of an ion channel,[7] and for a carbon nanotube.[3,6]

We were unable to find intermittent behavior when the water molecules were replaced by a reference OW system of oxygen atoms interacting only through the Lennard-Jones part of the SPC/E interaction potential between water molecules (the OW model). Further investigations would be needed to examine whether the apparently different behavior of these two systems can be reconciled, perhaps by a careful selection of the model parameters.

(b) The intermittent permeation can be understood as being due to transitions of the system between ''empty'' and ''filled'' states of the channel which correspond to the two minima in the grand potential $\Omega(n)$ of a subsystem including the channel, considered as a function of the number of molecules inside the channel, which plays the role of an ''order parameter'' (or ''reaction coordinate''), in a Landau free energy analysis. Transitions between the two states require the system to overcome the grand potential barrier which may be identified with the transition state. Intermittent behavior can be observed during the length of MD runs (typically a few ns) if the barrier is of the order of a few k_BT. When the radius of the channel shrinks, the minimum in $\Omega(n)$, corresponding to the filled state, eventually disappears [cf. Fig. 8(d)].

(c) In the filled state, water confined to a cylindrical pore exhibits a surprisingly bulklike behavior. The radial density profiles show little structure compared to the profiles for the OW model under comparable physical conditions. The mean density of water molecules inside the pore is close to its bulk value, while the diffusion constant along the cylinder axis is comparable to bulk diffusivity. The number of hydrogen bonds per molecule is close to 4 for molecules near the channel axis and only drops to a value around 2.5 near the channel surface.[12]

(d) The filling of a channel appears to be preceded by the formation of a ''percolating'' linear cluster of hydrogen bonded water molecules spanning the whole channel length. This percolating cluster may play a role similar to a critical nucleus in the nucleation of stable phases.

The behavior of water inside the present ion channel model shows important differences from that observed in recent simulations of a carbon nanotube of comparable dimensions,[3] even though in both cases pore filling is intermittent in time. Only single-file permeation occurs in the carbon nanotube, presumably due to the smaller radius and the highly hydrophobic nature of the tube wall. The intermit-

tency mechanism for the carbon nanotube appears to be well described by a confined lattice gas model.[29] The filled channel state in the present simulations, however, involves a much larger number of water molecules, which are far from being single file. We have been so far unable to map our water simulation system onto a simpler Lennard-Jones model.

While the grand potential profiles allow the calculation of the *probability* that a pore is filled, according to Eq. (15), this does not provide the *rate* at which ''transitions'' occur in equilibrium between the empty and filled states; according to the time-dependent occupation data in Figs. 5 and 6, this rate is of the order of 1 ns^{-1} near the threshold. The rate constant may be related to an equilibrium time-dependent correlation function,[30] and practical implemetations of such calculations in MD simulations are well documented.[28] Such calculations are currently under way.

Another extension of the present work which is being actively pursued is to physiologically more relevant nonequilibrium situations. Recent simulation work on simple models for ion channels investigates ion transport when a large external electric field is applied across the membrane.[31] We are presently considering the case where an ion channel links two reservoirs containing ionic solutions at different ionic strengths; this provides the natural driving force for ion transport. Preliminary results of the simulations will be published elsewhere.[32]

APPENDIX A: SIMULATION DETAILS

1. Wall potential

The interaction potential with the pore wall, $\phi_w(\mathbf{r})$, for a particle (with Lennard-Jones parameters ϵ_{part} and σ_{part}) well inside the cylindrical pore of radius R, at radial distance r from the pore axis, is identical to that which would be obtained if the particle were in an infinite cylindrical pore in a material made from ''smeared-out'' LJ particles at density ρ and with LJ parameters ϵ_{wall} and σ_{wall}. This interaction can be calculated by integrating the standard 12-6 LJ potential between the particle in the pore and those in the wall, over the whole infinite volume of the wall material. This calculation was done by Peterson *et al.*[15] Defining $\epsilon = \sqrt{\epsilon_{part}\epsilon_{wall}}$ and $\sigma = 1/2(\sigma_{part}+\sigma_{wall})$, $\phi_w(r)$ is given by

$$\phi_w(r) = \pi\rho\epsilon\left(\frac{7\sigma^{12}}{32}K_9(r) - \sigma^6 K_3(r)\right), \tag{A1}$$

where $K_m(r)$ is defined as

$$K_m(r) = R^{-m}\int_0^\pi d\theta[-\eta\cos\theta + (1-\eta^2\sin^2\theta)^{1/2}]^{-m}$$
$$= R^{-m}k_m(\eta) \tag{A2}$$

and $\eta = r/R$.

On the cylinder axis, $\phi_w(0) = \pi^2 n\epsilon(7\sigma^{12}/32R^9 - \sigma^6/R^3)$.

The resulting force in the radial direction, $F_w(r) = -d\phi_w/dr$, is

$$F_w(r) = -\pi n\epsilon\left(\frac{63\sigma^{12}}{32}J_{10}(r) - 3\sigma^6 J_4(r)\right), \tag{A3}$$

where $J_m(r)$ is given by

$$J_m(r) = R^{-m}\int_0^\pi d\theta[\cos\theta + \eta\sin^2\theta(1-\eta^2\sin^2\theta)^{-1/2}]$$
$$\times[-\eta\cos\theta + (1-\eta^2\sin^2\theta)^{1/2}]^{-m}$$
$$= R^{-m}j_m(\eta). \tag{A4}$$

The functions $k_3(\eta)$, $k_9(\eta)$, $j_4(\eta)$, and $j_{10}(\eta)$ are evaluated by numerical integration, tabulated for 10 000 values between 0 and 1, and stored in each simulation run. Interpolation between the values in these tables allows ϕ_w and F_w to be evaluated for any radial distance r.

For a particle outside the pore ($|z| > L/2$) and with $r > R$, situated a distance $d < R$ from either of the planar surfaces of the ''membrane,'' the interaction potential ϕ_w' is the same as in the pore, but with r replaced by $R-d$ and shifted by $\phi_w(0)$ to avoid a discontinuity at $d = R$:

$$\phi_w'(d) = \phi_w(R-d) - \phi_w(0). \tag{A5}$$

This potential is rounded at the pore edges for particles close to the pore mouth, with $|z| \gg L/2$, $r < R$ and $\zeta = \sqrt{d^2 + (R-r)^2} < R$: in this case the interaction is given by $\phi_w'(\zeta)$, and the resulting force has components in both the radial and axial directions.

As the particle enters the pore, its interaction with the pore walls changes smoothly to that given by ϕ_w: for particles with axial positions $L/2 - l < |z| < L/2$, the wall potential is given by

$$\phi_w''(r,z) = \phi_w(r) - \frac{\phi_w(0)}{2}$$
$$\times\left(1 \pm \tanh\left[\frac{10}{l}(z \mp L/2 \pm l/2)\right]\right). \tag{A6}$$

In these simulations, the LJ parameters used for the wall were those for a CH_3 group in a hydrocarbon chain: $\epsilon_{wall} = 0.8148\ \mathrm{kJ\,mol^{-1}}$, $\sigma_{wall} = 3.75$ Å (Ref. 14), $\rho = 0.033\ \text{Å}^{-3}$, and $l = 1$ Å.

2. Numerical implementation of the variational method for wall polarization

When the ''membrane'' region is polarizable, $\epsilon_{wall} > 1$, the induced polarization surface charge density $\rho_{pol}(\mathbf{s}) = \epsilon_0 h(\mathbf{s})$ is found by minimizing the variational functional $I_2[h]$ described in a previous paper.[18] The minimization method is as described in that paper. A grid is constructed on the wall surface: on the cylindrical pore surface the grid spacings Δz and $R\Delta\phi$ are such that $\Delta z \approx R\Delta\phi \approx 0.05$ nm, and on the planar surfaces, the grid points are arranged in a series of concentric circles, with spacings of ≈ 0.1 nm. The planar grids extend to a radius $R + 0.45$ nm. For a channel of radius $R = 0.6$ nm and length $L = 0.8$ nm, the total number of grid points is 1776 (1200 on the cylindrical surface and 288 each on the two planar surfaces).

The functional is evaluated on the grid as described in Ref. 18. Because the system is periodic in all three dimensions, we use the ''minimum image Green's function'' in x, y, and z:

$$G(\mathbf{s}_i-\mathbf{s}_j)=\frac{1}{4\pi\sqrt{a_x^2+a_y^2+a_z^2}}, \tag{A7}$$

where

$$a_x=(x_i-x_j)-L_x\mathrm{nint}\left(\frac{x_i-x_j}{L_x}\right), \tag{A8}$$

L_x being the cell length in the x direction and nint the nearest integer function. Equivalent expressions in y and z give a_y and a_z. The minimization is performed using a simple steepest-descent procedure.

The full minimization procedure is performed only once every 100 MD time steps. At intermediate time steps, $h(\mathbf{s})$ is updated by an approximate procedure. Using the notation of Ref. 18, we return to the case of a dielectric body with dielectric susceptibility $\chi(\mathbf{r})$, in which a polarization charge density $\rho_{pol}(\mathbf{r})=-\nabla\cdot\mathbf{P}(\mathbf{r})=\epsilon_0 h(\mathbf{r})$ is induced by an external potential $\psi_e(\mathbf{r})$ created by some fixed charge density $\rho(\mathbf{r})=\epsilon_0 g(\mathbf{r})$ outside the dielectric body. Defining $\psi_e(\mathbf{r})$ as in Ref. 18, $h(\mathbf{r})$ must satisfy the relation

$$h(\mathbf{r})=\nabla\cdot\left(\chi(\mathbf{r})\nabla\left[\psi_e(\mathbf{r})+\int d^3r' h(\mathbf{r}')G(\mathbf{r}-\mathbf{r}')\right]\right). \tag{A9}$$

Expanding this and using the relations $\nabla^2 G(\mathbf{r}-\mathbf{r}')=-\delta(\mathbf{r}-\mathbf{r}')$ and $\nabla^2\psi_e(\mathbf{r})=-g(\mathbf{r})$ leads to

$$h(\mathbf{r})(1+\chi(\mathbf{r}))=\nabla\chi\cdot\nabla\psi_e+\int d^3r' h(\mathbf{r}')\nabla\chi\cdot\nabla G(\mathbf{r}-\mathbf{r}'). \tag{A10}$$

For the case where the dielectric body is of a uniform susceptibility $\chi_{in}=\epsilon_{in}-1$, Eq. (A10) reduces to a surface expression, following the methods of Ref. 18:

$$\frac{(\epsilon_{in}+1)}{2}h(\mathbf{s})=(\epsilon_{in}-1)\left[\frac{\partial\psi_e}{\partial n}+\int d^2s' h(\mathbf{s}')\frac{\partial G(\mathbf{s}-\mathbf{s}')}{\partial n}\right], \tag{A11}$$

where $\partial/\partial n$ denotes a derivative in the direction normal to the surface, pointing into the dielectric body. In the case where there is also a finite susceptibility $\chi_{out}=\epsilon_{out}-1$ in the region surrounding the body, ϵ in Eq. (A11) is replaced by $\kappa=\epsilon_{in}/\epsilon_{out}$.

The approximate update of $h(\mathbf{s})$ simply consists in using the results of the previous timestep on the right-hand side of Eq. (A11):

$$\frac{(\epsilon_{in}+1)}{2}h_i^{t+\Delta t}=(\epsilon_{in}-1)\left[\frac{\partial\psi_e(\mathbf{s}_i)}{\partial n_i}+\sum_j a_j h_j^t\frac{\partial G(\mathbf{s}_i-\mathbf{s}_j)}{\partial n_i}\right], \tag{A12}$$

where h_i^t is the value of $h(\mathbf{s})$ at grid point i and time t, and a_i is the area associated with grid point i.

APPENDIX B: MEASUREMENT OF DIFFUSION CONSTANTS

The diffusion constant D for motion in one dimension (here along the pore, or z, axis) is usually obtained from the relation

$$\langle(z(t)-z(0))^2\rangle=2Dt. \tag{B1}$$

Equation (B1) holds strictly only for long times over which particle motion is diffusive: in practice $\langle(z(t)-z(0))^2\rangle$ is usually monitored over 50–100 ps and linear behavior sets in after $\sim$1 ps. Equation (B1) can be used in simulations of infinitely long pores,[33] but it fails for finite pores, if we include only particles which have positions $|z|<L/2$ both at times 0 and t in the average $\langle(z-z_0)^2\rangle$. In this case, $\langle(z-z_0)^2\rangle$ is no longer linear in time but rather shows saturation behavior.

Assuming that particles inside the pore of length L move purely diffusively in the z direction, the probability $p(z|z_0)$ that a particular particle which starts at position z_0 and is inside the pore at time t has position z at time t is

$$p(z|z_0)=\frac{2}{\sqrt{4\pi Dt}}\frac{e^{-(z-z_0)^2/4Dt}}{\left[\Phi\left(\frac{L/2-z_0}{\sqrt{4Dt}}\right)-\Phi\left(\frac{-L/2-z_0}{\sqrt{4Dt}}\right)\right]}, \tag{B2}$$

where $\Phi(x)$ is the error function: $\Phi(x)=(2/\sqrt{\pi})\int_0^x dy e^{-y^2}$. The denominator in Eq. (B2) arises from the need for $p(z|z_0)$ to be normalized over the length L of the pore. Assuming that the particles are uniformly distributed along the pore, $p(z_0)=1/L$. The average $\langle[z(t)-z(0)]^2\rangle$ is then given by

$$\langle(z-z_0)^2\rangle=\frac{1}{L}\int_{-L/2}^{L/2}dz_0\int_{-L/2}^{L/2}dz(z-z_0)^2 p(z|z_0). \tag{B3}$$

The integral (B3) may be partially calculated analytically to give

$$\langle(z-z_0)^2\rangle=2Dt+\frac{\sqrt{4Dt}}{L\sqrt{\pi}}\int_{-L/2}^{L/2}dz_0 F(z_0), \tag{B4}$$

where

$$F(z_0)=\frac{-(L/2-z_0)e^{-(L/2-z_0)^2/4Dt}+(-L/2-z_0)e^{-(-L/2-z_0)^2/4Dt}}{\Phi\left(\frac{L/2-z_0}{\sqrt{4Dt}}\right)-\Phi\left(\frac{-L/2-z_0}{\sqrt{4Dt}}\right)}. \tag{B5}$$

Expression (B4), which may be evaluated numerically, describes the time evolution of $\langle (z-z_0)^2 \rangle$ in a finite channel of length L, where only particles which are inside the channel at times 0 and t are included in the average. For an infinitely long channel, the second term vanishes and Eq. (B1) is recovered. Fitting Eq. (B4) to the measured simulation data allows D to be estimated.

Testing expression (B4) in the range $0<t<50$ ps for a sample of bulk OW particles in which only particles within a ''virtual'' slab of length L are included gives an excellent fit to the data. Reasonable fits are obtained for simulations of particles inside pores, where statistical errors are larger and deviations from diffusive behavior are more likely.

APPENDIX C: THE BIASING POTENTIAL

The form of the biasing potential used in this work is

$$W(n)/k_BT=(n-n_{\min})^{-12}+(n_{\max}-n)^{-12}+c_1n+c_2n^2+c_3n^3, \tag{C1}$$

where n is defined in Eq. (4). The first two terms in Eq. (C1) force the system to have a value of n in the range $n_{\min}<n<n_{\max}$ (assuming the run begins with n in this range). The coefficients c_1, c_2, and c_3 (which are different for each window) can be adjusted to achieve even sampling within the window. In practice these coefficients are determined either by extrapolation of the results for a previous window or simply by trial and error. The simulation time for each window must be long enough for good sampling of the phase space accessible to the system with values of n in the range $n_{\min}<n<n_{\max}$. In this work, the width $n_{\max}-n_{\min}$ of the windows was four molecules and the sampling time for each window was 200 ps. Overlapping windows were used, making it easier to join the results to form a profile and also enabling the starting configuration for a particular window to be obtained from one of the configurations generated in the previous run.

Each window sampling run gives a portion of the grand potential profile $\Omega(n)$, shifted by a value A which is different for each window, as described in Sec. V. Error bars are estimated by dividing each window sampling run of 200 ps into ten sections, each of length 20 ps and finding the variance of $P_{bias}(n)$ over the ten sections for each n value. The variance of $\Omega(n)$ is then found using Eq. (13).

The constants A_i in Eq. (13) are determined for each window i by fitting the grand potential profile to a polynomial in n.

APPENDIX D: A SIMPLE MODEL

In this section, a simple model for the free energy difference between the filled and empty channels, based on macroscopic arguments, is put forward and tested. This macroscopic model is motivated by the arguments of classical nucleation theory, in which the free energy of a critical nucleus formed is described in terms of surface and bulk contributions. We assume that the filled channel contains a cylinder of bulklike fluid of radius R_{eff} and length L_{eff}, which has a cylindrical interface with the wall, with surface free energy $\Omega_{cyl}=2\pi R_{\text{eff}}L_{\text{eff}}\gamma_{lw}$, γ_{lw} being the surface tension of the water–wall interface. The empty channel contains no water and in consequence there are two circular liquid–vapor interfaces at the ends of the channel (since the volume is here so small, the vacuum inside the channel is equivalent to vapor). The surface free energy in this case is $\Omega_{ends}=2\pi R_{\text{eff}}^2\gamma_{lv}$, where γ_{lv} is the surface tension of the liquid–vapor interface.

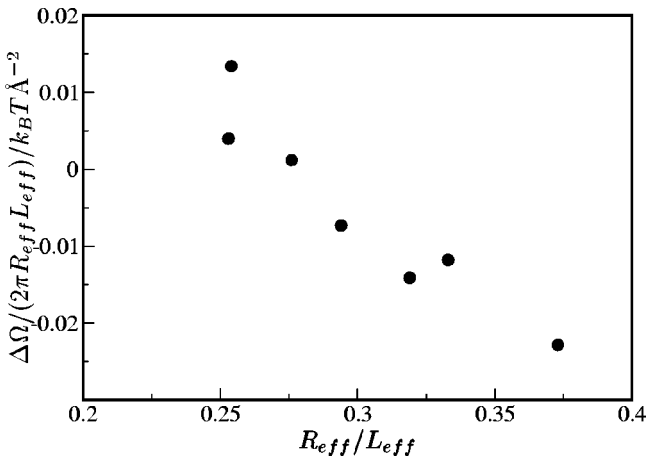

FIG. 14. $\Delta\Omega/2\pi R_{\text{eff}}L_{\text{eff}}$, in units of k_BT Å^{-2}, plotted as a function of $R_{\text{eff}}/L_{\text{eff}}$ for the channel geometries listed in Table III.

As discussed in Sec. V, a subsystem close to the channel is effectively simulated in the grand canonical ensemble. When the channel fills, therefore, an additional number of particles M enter the subsystem. Assuming that the same grand potential per particle, ω, can be associated with particles in the channel and in the reservoir, the grand potential change on channel filling is $\Delta\Omega=M\omega-\Omega_{ends}+\Omega_{cyl}$. However, under ambient conditions of density and temperature, $\omega=-Pv$, where $P\sim10^5$ Pa is the pressure and $v\sim30$ Å^3 is the volume per particle ω, is extremely small and can be neglected. This simple model therefore predicts that the grand potential difference between the filled and empty channel states, $\Delta\Omega$, is given by

$$\Delta\Omega=\Omega_{cyl}-\Omega_{ends}=2\pi R_{\text{eff}}L_{\text{eff}}\gamma_{lw}-2\pi R_{\text{eff}}^2\gamma_{lv} \tag{D1}$$

or, alternatively,

$$\frac{\Delta\Omega}{2\pi R_{\text{eff}}L_{\text{eff}}}=\gamma_{lw}-\frac{R_{\text{eff}}}{L_{\text{eff}}}\gamma_{lv}. \tag{D2}$$

Figure 14 shows values of $\Delta\Omega/(2\pi R_{\text{eff}}L_{\text{eff}})$, obtained from the grand potential profiles for a number of different channel geometries, with $R_{\text{eff}}=0.32-0.47$ nm and $L_{\text{eff}}=1.17-1.47$ nm, plotted against $R_{\text{eff}}/L_{\text{eff}}$. Fitting a linear profile to the results gives values for the two surface tensions: $\gamma_{lv}=0.26k_BT/\text{Å}^2=110$ mJ m^{-2} and $\gamma_{lw}=0.074k_BT/\text{Å}^2=30$ mJ m^{-2}. Experimental values of 72 mJ m^{-2} and 51 mJ m^{-2} for the surface tensions of the water liquid–vapor interface and the water–*n*-octane interface are quoted by Adamson and Gast[34] and by Israelachvili,[35] respectively. This is in reasonable agreement, given the simplistic nature of the model.

This simple model is similar in essence to that put forward by Maibaum and Chandler[29] to explain the rather different phenomenon of single-file filling of carbon nanotubes

by water. Here also the free energy difference between the empty and filled states is determined by the interfaces at the pore ends and the internal pore wall, respectively.

We note that our model does not explain the size or shape of the grand potential barrier to channel filling. This could only be done using surface energy arguments by making an assumption about the arrangement of water molecules in the channel during the filling process.

ACKNOWLEDGMENTS

The authors would like to thank S. Auer, P. Bolhuis, D. Chandler, D. Frenkel, and R. Lynden-Bell for their advice and suggestions. R.A. is grateful to EPSRC and to Unilever for funding.

[1] For a review, see L. D. Gelb, K. E. Gubbins, R. Radhakrishnan, and M. Sliwinska-Bartkowiak, Rep. Prog. Phys. **62**, 1573 (1999).
[2] B. Smit, J. Phys. Chem. **99**, 5597 (1995).
[3] G. Hummer, J. C. Rasaiah, and J. P. Nowortya, Nature (London) **414**, 188 (2001).
[4] M. Wilson and P. A. Madden, J. Am. Chem. Soc. **125**, 2101 (2001).
[5] See, e.g., B. Hille, *Ionic Channels of Excitable Membranes*, 2nd ed. (Sinauer, Sunderland, MA, 1992).
[6] A. Waghe, J. C. Rasaiah, and G. Hummer, J. Chem. Phys. **117**, 10789 (2002).
[7] O. Beckstein, P. C. Biggin, and M. S. P. Sansom, J. Phys. Chem. B **105**, 12902 (2001).
[8] R. Allen, S. Melchionna, and J.-P. Hansen, Phys. Rev. Lett. **89**, 175502 (2002).
[9] Y. Zhou, J. H. Morais-Cabral, A. Kaufman, and R. MacKinnon, Nature (London) **414**, 43 (2001).
[10] S. Bernèche, J. H. Morais-Cabral, A. Kaufman, and R. MacKinnon, Nature (London) **414**, 43 (2001).
[11] For a recent review, see D. P. Tieleman, P. C. Biggin, G. R. Smith, and M. S. P. Sansom, Q. Rev. Biophys. **34**, 473 (2001).
[12] R. Allen, S. Melchionna, and J.-P. Hansen, J. Phys.: Condens. Matter **15**, S297 (2003).
[13] H. J. C. Berendsen, J. R. Grigera, and T. P. Straatsma, J. Phys. Chem. **91**, 6269 (1987).
[14] M. G. Martin and J. I. Siepmann, J. Phys. Chem. B **102**, 2569 (1998).
[15] B. K. Peterson, J. P. R. B. Walton, and K. E. Gubbins, J. Chem. Soc., Faraday Trans. 2 **82**, 1789 (1986).
[16] See, e.g., J. D. Jackson, *Classical Electrodynamics*, 3rd ed. (Wiley, New York, 1999).
[17] R. Allen and J.-P. Hansen, Mol. Phys. **101**, 1575 (2003).
[18] R. Allen, J.-P. Hansen, and S. Melchionna, Phys. Chem. Chem. Phys. **3**, 4177 (2001).
[19] All simulations were performed using the package DL_PROTEIN, written by S. Melchionna and S. Cozzini: S. Melchionna, and S. Cozzini, *DL_Protein 2.1 User Guide*, 2001.
[20] H. J. C. Berendsen, J. P. M. Postma, W. F. van Gunsteren, A. DiNola, and J. R. Haak, J. Chem. Phys. **81**, 3684 (1984).
[21] U. Essmann, L. Perera, M. Berkowitz, T. Darden, H. Lee, and L. G. Pedersen, J. Chem. Phys. **103**, 8577 (1995).
[22] J.-P. Hansen and L. Verlet, Phys. Rev. **184**, 151 (1969).
[23] A. Lotfi, J. Vrabec, and J. Fischer, Mol. Phys. **76**, 1319 (1992).
[24] C. Y. Lee, J. A. McCammon, and P. J. Rossky, J. Chem. Phys. **80**, 4448 (1984); S. H. Lee and P. J. Rossky, *ibid.* **100**, 3334 (1994).
[25] W. L. Jorgensen, J. Chandrasekhar, J. D. Madura, R. W. Impey, and M. L. Klein, J. Chem. Phys. **79**, 926 (1983).
[26] U. Raviv, P. Laurat, and J. Klein, Nature (London) **413**, 51 (2001).
[27] J. C. Shelley and G. N. Patey, J. Chem. Phys. **102**, 7656 (1995).
[28] See, e.g., D. Frenkel and B. Smit, *Understanding Molecular Simulation*, 2nd ed. (Academic, London, 2002).
[29] L. Maibaum and D. Chandler, J. Phys. Chem. B **107**, 1189 (2003).
[30] See, e.g., G. Ciccotti and M. Ferrario, in *Monte Carlo and Molecular Dynamics of Condensed Matter Systems*, edited by K. Binder and G. Ciccotti (Italian Physical Society, Bologna, 1996).
[31] See, e.g., P. S. Crozier *et al.*, Phys. Rev. Lett. **86**, 2467 (2001).
[32] J. Dzubiella, R. Allen, and J.-P. Hansen (unpublished).
[33] R. Lynden-Bell and J. Rasaiah, J. Chem. Phys. **105**, 9266 (1996).
[34] A. W. Adamson and A. P. Gast, *Physical Chemistry of Surfaces*, 6th ed. (Wiley, New York, 1997).
[35] J. Israelachvili, *Intermolecular and Surface Forces*, 2nd ed. (Academic, London, 1992).